

Criticality-Based Quantum Metrology in the Presence of Decoherence

Wan-Ting He, Cong-Wei Lu, Yi-Xuan Yao, Hai-Yuan Zhu, and Qing Ai*

Department of Physics, Applied Optics Beijing Area Major Laboratory,

Beijing Normal University, Beijing 100875, China

(Dated: September 23, 2022)

Quantum metrology aims to use quantum resources to improve the precision of measurement. Because quantum systems with criticality are very sensitive to the variation of order parameters around the quantum phase transition (QPT), quantum criticality has been presented as a novel and efficient resource. Generally, protocols of criticality-based quantum metrology often work without decoherence. In this paper, we address the issue whether the divergent feature of the inverted variance is indeed realizable in the presence of noise when approaching the QPT. Taking the quantum Rabi model (QRM) as an example, we obtain the analytical result for the inverted variance. We show that the inverted variance may be convergent in time due to the noise. When approaching the critical point, the maximum inverted variance demonstrates a power-law increase with the exponent -1.2 , of which the absolute value is smaller than that for the noise-free case, i.e., 2 . We also observe a power-law dependence of the maximum inverted variance on the relaxation rate and the temperature. Since the precision of the metrology is very sensitive to the noise, as a remedy, we propose performing the squeezing operation on the initial state to improve the precision under decoherence. In addition, we also investigate the criticality-based metrology under the influence of the two-photon relaxation. Contrary to the single-photon relaxation, the quantum dynamics of the inverted variance shows a completely-different behavior. It does not oscillate with the same frequency with respect to the re-scaled time for different dimensionless coupling strengths. Strikingly, although the maximum inverted variance still manifests a power-law dependence on the energy gap, the exponent is positive and depends on the dimensionless coupling strength. This observation implies that the criticality may not enhance but weaken the precision in the presence of two-photon relaxation. It can be well described by the non-linearity introduced by the two-photon relaxation.

I. INTRODUCTION

Quantum criticality has been shown to provide significant advantages for quantum sensing and metrology [1–10]. In quantum phase transition (QPT), a small variation in the order parameter may cause a huge change in the system’s properties when approaching the quantum critical point [11–13]. Thus, quantum criticality can be viewed as a valuable resource to acquire an ultrahigh-precision estimation. In the last few years, criticality-based quantum metrological schemes have gained increasing attention among both theoretical and experimental researchers. Many criticality-based quantum metrology protocols in QPT systems have been proposed, which can be classified into two types [4, 5]. One of them focuses on the critical behaviors of the QPT at equilibrium, and utilizes the ground state of the Hamiltonian near the critical point. Unfortunately, it is very inefficient to prepare the ground-state around the critical point by the state-of-art technology. The other focuses on the dynamical behaviors, which evolve under a Hamiltonian close to the critical point. It is quite similar to the interferometric paradigm in the typical quantum metrology. Previous work [3] has revealed that both two kinds of approaches yield the same scaling for a broad class of quantum many-body systems. Recently, a dynamic framework for criticality-based quantum metrol-

ogy, which preliminarily focuses on the dynamical approach, has been proposed [2, 14, 15]. The fundamental idea as well as the details of experimental implementation using quantum Rabi model (QRM) have been illustrated. The QRM is one of the most fundamental models describing quantum light-matter interactions [16]. There exists a superradiant QPT in the thermodynamic limit of the QRM [17–20]. The thermodynamic limit can be achieved when the reduced Rabi frequency approaches infinity in some quantum systems with criticality, such as the Dicke model, the Lipkin-Meshkov-Glick model and the QRM [5].

On the other hand, any quantum system inevitably suffers from the interaction with the surrounding environment and thus forms an open quantum system. It has been known over two decades that the quantum metrology with the maximum-entangled states shows no advantage over the classical counterpart when the decoherence is present [21]. Interestingly, when placed in a non-Markovian environment, the entangled probes indeed manifest their superiority by the quantum Zeno effect [22–26], and recently it was experimentally demonstrated by an exact and efficient quantum simulation approach [27–32].

In this work, inspired by the above discoveries, we analyze the achievable precision in the QRM when considering the thermal relaxation. The upper bound on the achievable precision of the metrology will be dramatically reduced owing to the noise. This result indicates that the dissipation poses severe limitations and thus hinders the metrological advantages in this framework. Furthermore,

* aiqing@bnu.edu.cn

we find that the inverted variance may converge in time no matter as a result of the noise. We further explore optimization of initial state and find that the precision can be improved by a squeezing operation on the initial state. On the other hand, recently two-photon relaxation has been experimentally realized [33]. It was theoretically shown that the two-photon relaxation preserves the Z_2 symmetry of the QRM. The initial states with even-odd parity manifest qualitatively distinct transient and steady state behaviors, which is present both at ultrastrong and weak couplings [34]. Motivated by these observations, we theoretically investigate the quantum dynamics of the metrology in the presence of two-photon relaxation.

This paper is organized as follows. In Sec. II, we outline some basic concepts in the quantum metrology based on the criticality and introduce the QRM with noise. In Sec. III, we analyze the results by the semiclassical equation of motion and discuss the effects of various physical parameters on the measurement precision. In Sec. IV, we investigate the effects of the two-photon relaxation on the metrology. The main conclusions of this paper are drawn in Sec. V.

II. MODEL

In this paper, we consider the QRM for criticality-based quantum metrology, which consists of a two-level system coupled to a single cavity mode. It is the most simplified version of the Dicke model [35]. The Hamiltonian of the QRM is

$$H_{\text{Rabi}} = \omega a^\dagger a + \frac{\omega_0}{2} \sigma_z - \lambda(a + a^\dagger)\sigma_x, \quad (1)$$

where ω is the frequency of the bosonic field, a^\dagger and a are the creation and annihilation operators of the field, ω_0 is the transition frequency of the two-level atom, σ_α ($\alpha = x, y, z$) are the Pauli operators of the atom, λ is the coupling strength. Let $g = 2\lambda/\sqrt{\omega\omega_0}$ be the dimensionless coupling constant. When the ratio of two transition frequencies diverges, i.e., $\eta = \omega_0/\omega \rightarrow \infty$, the energy gap closes and there exhibits a second-order normal-to-superradiant QPT at the critical point $g = 1$ [17]. In the limit of $\eta \rightarrow \infty$, through the Schrieffer-Wolff transformation $U_{\text{np}} = \exp[g\sqrt{\eta^{-1}}(a + a^\dagger)(\sigma_+ - \sigma_-)/2]$ [36], we can obtain an effective low-energy normal-phase Hamiltonian as

$$H_{\text{np}} = \omega[P^2 + (1 - g^2)X^2]/2, \quad (2)$$

where $X = (a + a^\dagger)/\sqrt{2}$ and $P = i(a^\dagger - a)/\sqrt{2}$ are the quadrature operators. Let $H_0 = \omega P^2/2$ and $H_1 = \omega X^2/2$. The quantum Fisher information (QFI) for the estimation of the parameter g around the critical point can be expressed as [2]

$$\mathcal{F}_g \simeq 16g^2 \frac{[\sin(\sqrt{\Delta_g}\omega t) - \sqrt{\Delta_g}\omega t]^2}{\Delta_g^3} \text{Var}(P^2)_{|\psi\rangle}, \quad (3)$$

where $\Delta_g = 4(1 - g^2)$ characterizes the energy gap, $\text{Var}(P^2)_{|\psi\rangle} = \langle\psi|P^2|\psi\rangle - \langle\psi|P|\psi\rangle^2$ is the variance of the momentum in the state $|\psi\rangle$. In experiments, the precision of measurement is characterized by the inverted variance as $F_g = \chi_g^2/(\Delta X)^2$ with $\chi_g = \partial_g\langle X \rangle$ and $(\Delta X)^2 = \langle X^2 \rangle - \langle X \rangle^2$. Here, $\langle X \rangle$ is the expectation of X . Assume an initial state $|\psi(0)\rangle = |\downarrow\rangle \otimes |\psi\rangle_b$ with the spin in the spin-down state $|\downarrow\rangle$ and the bosonic field state $|\psi\rangle_b = (|0\rangle + i|1\rangle)/\sqrt{2}$. The inverted variance will achieve its local maxima $F_g(\tau) = \chi_g^2/(\Delta X)^2|_{t=\tau} = 8g^2\omega^2\Delta_g^{-2}\tau^2$ at $\tau = 2m\pi/(\sqrt{\Delta_g}\omega)$ with $m \in \mathbb{Z}$. Notice that the inverted variance diverges in the long-time limit. The QFI at the same time is $\mathcal{F}_g(\tau) \simeq 16g^2\omega^2\Delta_g^{-2}\tau^2\text{Var}(P^2)_{|\psi\rangle_b}$. The local maximum of the inverted variance $F_g(\tau)$ is of the same order of the QFI $\mathcal{F}_g(\tau)$.

III. SINGLE-PHOTON RELAXATION

First of all, we consider the QRM with the single-photon relaxation. The inverted variance can be obtained solving the Lindblad-form master equation numerically by using QuTip [37–39]. In the $\eta \rightarrow \infty$ limit, all the corrections which have an order higher than $\eta^{-1/2}$ become zero. Thus, we have

$$U_{\text{np}}^\dagger a U_{\text{np}} \approx a. \quad (4)$$

Upon the projection onto the spin-down subspace, we obtain the effective master equation $\dot{\rho} = -i[H_{\text{np}}, \rho] + \gamma_a D[a] + \gamma_h D[a^\dagger]$, where $D[a] = a\rho a^\dagger - a^\dagger a\rho/2 - \rho a^\dagger a/2$, γ_a is the decay rate, γ_h is the heating rate [40]. Applying a semiclassical equation of motion for the open QRM [41, 42], we have

$$\begin{aligned} \frac{d}{dt}\langle X \rangle &= -\frac{\gamma_a - \gamma_h}{2}\langle X \rangle + \omega\langle P \rangle, \\ \frac{d}{dt}\langle P \rangle &= -\frac{\gamma_a - \gamma_h}{2}\langle P \rangle - \frac{\Delta_g\omega}{4}\langle X \rangle, \\ \frac{d}{dt}\langle X^2 \rangle &= -(\gamma_a - \gamma_h)\langle X^2 \rangle + \omega\langle G \rangle + \frac{\gamma_a + \gamma_h}{2}, \\ \frac{d}{dt}\langle P^2 \rangle &= -(\gamma_a - \gamma_h)\langle P^2 \rangle - \frac{\Delta_g\omega}{4}\langle G \rangle + \frac{\gamma_a + \gamma_h}{2}, \\ \frac{d}{dt}\langle G \rangle &= -(\gamma_a - \gamma_h)\langle G \rangle + 2\omega\langle P^2 \rangle - \frac{\Delta_g\omega}{2}\langle X^2 \rangle, \end{aligned} \quad (5)$$

where $\langle \cdot \rangle = \text{Tr}(\cdot\rho_b)$ with ρ_b being the density matrix of the bosonic field and $G = XP + PX$. In general, $\gamma_a = \kappa(\bar{n} + 1)$ and $\gamma_h = \kappa\bar{n}$ describe the coupling of the field to a thermal reservoir at temperature T with mean number

$$\bar{n} = \frac{1}{e^{\omega/k_B T} - 1} \quad (6)$$

of thermal photons, k_B the Boltzmann constant, κ the decay rate at zero temperature [40]. By solving Eq. (5), the inverted variance $F_g(t)$ is analytically given as

$$F_g(t) = \frac{4\Delta_g^{-2}(4 - \Delta_g)A^2(t)}{B(t) + \frac{2n+1}{\Delta_g\omega^2 + \kappa^2}C(t)}, \quad (7)$$

where the three time-dependent factors are respectively

$$\begin{aligned} A(t) &= [\Delta_g \omega t \langle X(0) \rangle + 4 \langle P(0) \rangle] \sin\left(\frac{1}{2} \sqrt{\Delta_g} \omega t\right) \\ &\quad - 2 \sqrt{\Delta_g} \omega t \langle P(0) \rangle \cos\left(\frac{1}{2} \sqrt{\Delta_g} \omega t\right), \end{aligned} \quad (8)$$

$$\begin{aligned} B(t) &= 2\Delta_g [1 + \cos(\sqrt{\Delta_g} \omega t)] \text{Var}(X^2)_{|\psi(0)} \\ &\quad + 8[1 - \cos(\sqrt{\Delta_g} \omega t)] \text{Var}(P^2)_{|\psi(0)} \\ &\quad + 8\sqrt{\Delta_g} \sin(\sqrt{\Delta_g} \omega t) \text{Re}[\text{Cov}(X, P)], \end{aligned} \quad (9)$$

$$\begin{aligned} C(t) &= \Delta_g (\Delta_g \omega^2 + 4\omega^2 + 2\kappa^2) (e^{\kappa t} - 1) - (4 - \Delta_g) \times \\ &\quad \kappa^2 [1 - \cos(\sqrt{\Delta_g} \omega t)] + \sqrt{\Delta_g} \omega \kappa \sin(\sqrt{\Delta_g} \omega t). \end{aligned} \quad (10)$$

Here, $\langle X(0) \rangle$ and $\langle P(0) \rangle$ are the expectation values of the position and momentum operators over the initial state of the bosonic field $|\psi(0)\rangle$, $\text{Cov}(X, P) = \langle\psi(0)|XP|\psi(0)\rangle - \langle\psi(0)|X|\psi(0)\rangle\langle\psi(0)|P|\psi(0)\rangle$. When the noise is absent, i.e., $\kappa = 0$, it can be proven that the local maxima of the inverted variance at the evolution time $\tau = 2m\pi/(\sqrt{\Delta_g}\omega)$ is equal to $16g^2\omega^2\Delta_g^{-2}\tau^2 \langle P(0) \rangle^2 / (\Delta X(0))^2$. It scales quadratically with τ , and shows a divergent feature when approaching the critical point, i.e., $F_g(\tau) \propto \Delta_g^{-3} \rightarrow \infty$.

At zero temperature, the average photon number \bar{n} equals zero. In this case, we assume the same initial state $(|0\rangle + i|1\rangle)/\sqrt{2}$ as Ref. [4]. Figure 1 shows the inverted variance of the QRM close to the critical point when coupling with a thermal reservoir at zero temperature. As shown in Fig. 1(a), the dynamics of $F_g(t)$ manifest abundant phenomena. At first, the envelope increases along with the increase of the time. Then, after passing the maximum, it decreases and converges due to the noise. It is in sharp contrast to the prediction when the noise is absent. Furthermore, we also investigate the maximum values of $F_g(t)$ for different κ 's in Fig. 1(b). As shown by the numerical fitting, the dependence of the maximum inverted variance $F_g(t)|_{\max}$ on κ can be well described by $a\kappa^b$. For different g 's, although a 's are distinct, all b 's are non-exceptionally equal to 2.

In Fig. 2(a), we plot the time dependence of $F_g(t)$ near the critical point for different g 's. Notice that the time is rescaled by $\Delta_g \omega / 2\pi$, which is approximately the oscillating frequency of $F_g(t)$ for small $\kappa \ll \omega$. Similarly as in Fig. 1(a), we can see that $F_g(t)$ gradually increase from their initial values $F_g(0) = 0$ to the maximum values. Then, $F_g(t)$ begins to decrease and eventually vanishes in the long-time limit. By theoretically obtaining $F_g(t)$ under different κ 's, we plot the relation of the maximum of $F_g(t)$ with respect to Δ_g in Fig. 2(b). We can see that $F_g(t)$ decays as Δ_g increases for a given κ . It indicates that the noise hinders the metrological advantages in this framework. Again, we numerically fit the maximum of $F_g(t)$ as a function of Δ_g , i.e., $a\Delta_g^b$. Despite of different a 's, all curves consistently decay with a nearly-identical $b \simeq -1.18 > -2$, which is the noise-free case. This implies that in the noisy QRM, the inverted variance still diverges when approaching the critical point, i.e., $\Delta_g \rightarrow 0$. In other words, by the scaling behavior, we

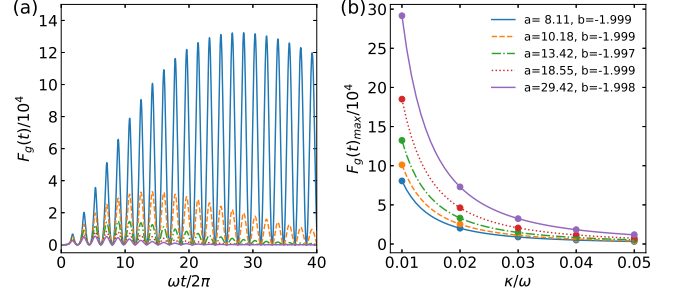


Figure 1. The effect of the noise strength κ on the precision of the criticality-enhanced metrology. (a) The inverted variance of the QRM in the vicinity of the critical point, e.g. $g = 0.96$, when coupling with a thermal reservoir at zero temperature, for $100\kappa/\omega = 1, 2, 3, 4, 5$. They correspond to the blue solid, orange dashed, green dash-dotted, red dotted, purple solid line, respectively. (b) The maximum of the inverted variance as a function of the noise parameter κ . From the bottom to the top, the five curves correspond to $g = 0.94, 0.95, 0.96, 0.97, 0.98$, respectively. The dots are obtained from the master equation, while the curves are calculated by the numerical fitting.

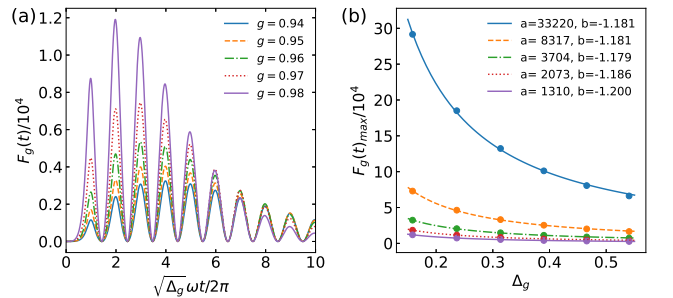


Figure 2. The effect of the energy gap Δ_g on the precision of the criticality-enhanced metrology. (a) The inverted variance F_g of the QRM when approaching the critical point, e.g. $g = 0.94, 0.95, 0.96, 0.97, 0.98$, with the noise parameter $\kappa = 0.05\omega$. It is plotted against the rescaled time $\Delta_g \omega t / 2\pi$ to highlight the behavior that in the representation of the rescaled time F_g 's oscillate with the same frequency for different g 's. (b) The maximum of F_g vs Δ_g for $100\kappa/\omega = 1, 2, 3, 4, 5$, which correspond to the curves from the top to the bottom. The dots are obtained from the master equation, while the curves are calculated by the numerical fitting.

theoretically prove that the criticality-based metrology is robust in the presence of single-photon relaxation.

We now investigate the influence of average photon number. As it can be seen from Fig. 3(a), the time-rescaled $F_g(t)$'s for different g 's reach their local maxima at the same period while maximum values of $F_g(t)$ decay as \bar{n} increases. Again, we plot the maximum $F_g(t)$ vs the temperature T in Fig. 3(b). It's shown that the maximum $F_g(t)$ drops dramatically as T rises. This observation reminds us that although the criticality-based metrology

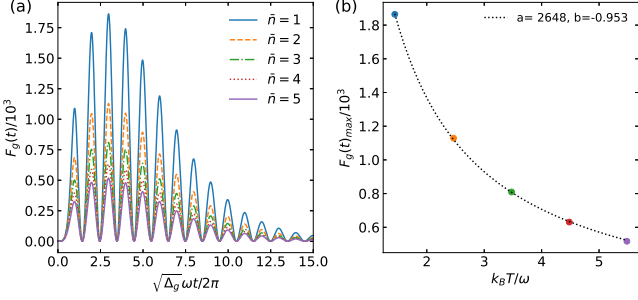


Figure 3. The effect of the temperature T on the precision of the criticality-enhanced metrology. (a) The inverted variance of the QRM close to the critical point, at $g = 0.96$, with $\bar{n} = 1, 2, 3, 4, 5$ and $\kappa/\omega = 0.05$. (b) The maximum inverted variance vs the temperature T . The black dotted line is numerically fitted by $a(k_B T/\omega)^b$ with $a = 2648$ and $b = -0.953$.

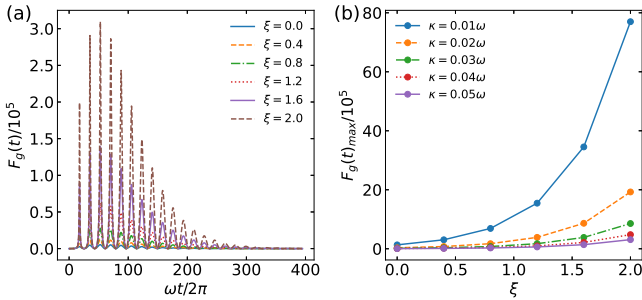


Figure 4. Improving the precision by performing a squeezing operation on the initial state. (a) $F_g(t)$ versus time t , with different squeezing parameter ξ , when $g = 0.96$ and $\kappa/\omega = 0.05$. (b) The maximum of F_g at different ξ 's with $100\kappa/\omega = 1, 2, 3, 4, 5$.

seems immune to the noise, the precision is very sensitive to the temperature. Hereafter, we will propose some method to relieve this disadvantage.

According to Eq. (7), the measurement accuracy highly depends on the initial state. This observation inspires us to perform a squeezing operation, defined by a squeezing operator $S(\xi) = \exp[(\xi^* a^2 - \xi a^{\dagger 2})/2]$, on the initial bosonic field state, where ξ is the squeezing parameter. As seen in Fig. 4, the maximum of $F_g(t)$ is significantly increased as ξ is enlarged. Although this gain can not completely offset the influence of decoherence, it offers an alternative way to improve the precision under decoherence.

IV. TWO-PHOTON RELAXATION

In the above investigations, we explore the quantum metrology in the presence of single-photon relaxation. However, the quantum dynamics of the QRM with single-photon and two-photon relaxation are totally different

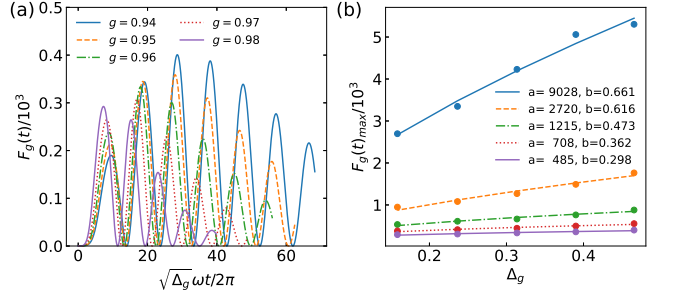


Figure 5. The effects of the two-photon relaxation. (a) The inverted variance F_g of the QRM when approaching the critical point, e.g. $g = 0.94, 0.95, 0.96, 0.97, 0.98$, with the noise parameter $\kappa = 0.05\omega$. It is plotted against the rescaled time $\sqrt{1 - g^2 \omega t / \pi}$. (b) The maximum of F_g at different g 's with $100\kappa/\omega = 1, 2, 3, 4, 5$. The dots are obtained from the master equation, while the curves are calculated by the numerical fitting.

[34]. Inspired by this discovery, we study the quantum metrology in the QRM with two-photon relaxation, which can be described by the effective master equation $\dot{\rho} = -i[H_{\text{np}}, \rho] + \gamma_a D[a^2] + \gamma_h D[a^{\dagger 2}]$ [34].

In Fig. 5(a), we investigate the dynamics of the inverted variance for different g 's under the influence of the two-photon relaxation. In contrast to the case with the single-photon relaxation, the quantum dynamics for different g 's do not oscillate with the same frequency for the rescaled time. In addition, as g increases, the time to achieve the maximum becomes shorter and shorter. Moreover, we plot the maximum inverted variance as a function of Δ_g in Fig. 5(b). Interestingly, the behavior is quite different from that for the single-photon relaxation in Fig. 1(b). The maximum inverted variance increases monotonically as Δ_g is enlarged. We again numerically fit the data with the function ax^b and thus obtain $a = 9.03 \times 10^3$ and $b = 0.661$ for $\kappa = 0.01\omega$. As κ increases, both a and b reduce dramatically. In other words, when we strengthen the noise, the inverted variance becomes smaller and shows weaker dependence on Δ_g . This remarkable difference can be well described by the Schrödinger equation with a non-Hermitian Hamiltonian [43, 44], when the relaxation rate is weak. When there is only single-photon relaxation, the non-Hermitian Hamiltonian is the original Hamiltonian H_{np} plus $-i(\gamma_a a^\dagger a + \gamma_h a a^\dagger)/2$. Although the Hamiltonian is non-Hermitian, the energy spectrum is still equally-spaced, which is fundamentally required by the criticality-based metrology [2]. However, for the case with two-photon relaxation, the non-Hermitian Hamiltonian is the original Hamiltonian H_{np} plus $-i(\gamma_a a^{\dagger 2} a^2 + \gamma_h a^2 a^{\dagger 2})/2$. Due to the non-linearity introduced by the two-photon relaxation, the energy spectrum is not equally-spaced and thus breaks down the underlying physical mechanism of the criticality-based metrology.

V. CONCLUSION

We have investigated the impact of decoherence on the criticality-based quantum metrology in the QRM, showing that the achieved precision still diverges when approaching the criticality. In particular, we consider the single-photon relaxation described by the Lindblad-form master equation. By the semiclassical equation of motion, we obtain the analytical solution for the precision characterized by the maximum inverted variance. We have shown that the precision is very sensitive to the temperature. As a remedy, we propose to improve

the precision by performing the squeezing operation on the initial state. Furthermore, we also investigate the performance of the metrology in the presence of two-photon relaxation. In contrast to the single-photon relaxation, the inverted variance do not oscillate against the rescaled time at the same frequency for different g 's. More strikingly, the maximum inverted variance shows a completely-different tendency when closing to the quantum phase transition.

This work is supported by Beijing Natural Science Foundation under Grant No. 1202017 and the National Natural Science Foundation of China under Grant Nos. 11674033, 11505007, and Beijing Normal University under Grant No. 2022129.

-
- [1] T. L. Heugel, M. Biondi, O. Zilberberg, and R. Chitra, Quantum Transducer Using a Parametric Driven-Dissipative Phase Transition, *Phys. Rev. Lett.* **123**, 173601 (2019).
- [2] Y. Chu, S. Zhang, B. Yu, and J. Cai, Dynamic Framework for Criticality-Enhanced Quantum Sensing, *Phys. Rev. Lett.* **126**, 010502 (2021).
- [3] M. M. Rams, P. Sierant, O. Dutta, P. Horodecki, and J. Zakrzewski, At the Limits of Criticality-Based Quantum Metrology: Apparent Super-Heisenberg Scaling Revisited, *Phys. Rev. X* **8**, 021022 (2018).
- [4] L. Garbe, M. Bina, A. Keller, M. G. A. Paris, and S. Felicetti, Critical Quantum Metrology with a Finite-Component Quantum Phase Transition, *Phys. Rev. Lett.* **124**, 120504 (2020).
- [5] S. Felicetti and A. Le Boite, Universal Spectral Features of Ultrastrongly Coupled Systems, *Phys. Rev. Lett.* **124**, 040404 (2020).
- [6] T. Ilias, D. Yang, S. F. Huelga, and M. B. Plenio, Criticality-Enhanced Quantum Sensing via Continuous Measurement, *PRX Quantum* **3**, 010354 (2022).
- [7] P. Zanardi, M. G. A. Paris, and L. C. Venuti, Quantum Criticality as a Resource for Quantum Estimation, *Phys. Rev. A* **78**, 042105 (2008).
- [8] M. Tsang, Quantum Transition-Edge Detectors, *Phys. Rev. A* **88**, 021801 (2013).
- [9] S. Fernández-Lorenzo and D. Porras, Quantum sensing close to a dissipative phase transition: Symmetry Breaking and Criticality as Metrological Resources, *Phys. Rev. A* **96**, 013817 (2017).
- [10] K. Gietka, F. Metz, T. Keller, and J. Li, Adiabatic Critical Quantum Metrology Cannot Reach the Heisenberg Limit even when Shortcuts to Adiabaticity are Applied, *Quantum* **5**, 489 (2021).
- [11] S. Sachdev, *Quantum Phase Transitions* (Cambridge University Press, UK, 2011).
- [12] H. T. Quan, Z. Song, X. F. Liu, P. Zanardi, and C. P. Sun, Decay of Loschmidt Echo Enhanced by Quantum Criticality, *Phys. Rev. Lett.* **96**, 140604 (2006).
- [13] Q. Ai, Y. D. Wang, G. L. Long, and C. P. Sun, Two Mode Photon Bunching Effect as Witness of Quantum Criticality in Circuit QED, *Sci. China Ser. G* **52**, 1898 (2009).
- [14] S. S. Pang and A. N. Jordan, Optimal Adaptive Control for Quantum Metrology with Time-Dependent Hamiltonians, *Nat. Commun.* **8**, 14695 (2017).
- [15] S. Pang and T. A. Brun, Quantum Metrology for a General Hamiltonian Parameter, *Phys. Rev. A* **90**, 022117 (2014).
- [16] M. O. Scully and M. S. Zubairy, *Quantum Optics* (Cambridge University Press, UK, 1997).
- [17] M.-J. Hwang, R. Puebla, and M. B. Plenio, Quantum Phase Transition and Universal Dynamics in the Rabi Model, *Phys. Rev. Lett.* **115**, 180404 (2015).
- [18] R. Puebla, M.-J. Hwang, J. Casanova, and M. B. Plenio, Probing the Dynamics of a Superradiant Quantum Phase Transition with a Single Trapped Ion, *Phys. Rev. Lett.* **118**, 073001 (2017).
- [19] J. S. Pedernales, I. Lizuain, S. Felicetti, G. Romero, L. Lamata, and E. Solano, Quantum Rabi Model with Trapped Ions, *Sci. Rep.* **5**, 15472 (2015).
- [20] D. Lv, S. An, Z. Liu, J.-N. Zhang, J. S. Pedernales, L. Lamata, E. Solano, and K. Kim, Quantum Simulation of the Quantum Rabi Model in a Trapped Ion, *Phys. Rev. X* **8**, 021027 (2018).
- [21] S. F. Huelga, C. Macchiavello, T. Pellizzari, A. K. Ekert, M. B. Plenio, and J. I. Cirac, Improvement of Frequency Standards with Quantum Entanglement, *Phys. Rev. Lett.* **79**, 3865 (1997).
- [22] A. W. Chin, S. F. Huelga, and M. B. Plenio, Quantum Metrology in Non-Markovian Environments, *Phys. Rev. Lett.* **109**, 233601 (2012).
- [23] A. G. Kofman, S. Ashhab, and F. Nori, Nonperturbative Theory of Weak Pre- and Post-Selected Measurements, *Phys. Rep.* **520**, 43 (2012).
- [24] Q. Ai, Y. Li, H. Zheng, and C. P. Sun, Quantum Anti-Zeno Effect without Rotating Wave Approximation, *Phys. Rev. A* **81**, 042116 (2010).
- [25] Q. Ai, D. Xu, S. Yi, A. G. Kofman, C. P. Sun, and F. Nori, Quantum Anti-Zeno Effect without Wave Function Reduction, *Sci. Rep.* **3**, 1752 (2013).
- [26] P. M. Harrington, J. T. Monroe, and K. W. Murch, Quantum Zeno Effects from Measurement Controlled Qubit-Bath Interactions, *Phys. Rev. Lett.* **118**, 240401 (2017).
- [27] X.-Y. Long, W.-T. He, N.-N. Zhang, K. Tang, Z.-D. Lin, H.-F. Liu, X.-F. Nie, G.-R. Feng, J. Li, T. Xin, Q. Ai, and D. W. Lu, Entanglement-Enhanced Quantum Metrology in Colored Noise by Quantum Zeno Ef-

- fect, *Phys. Rev. Lett.* **129**, 070502 (2022).
- [28] I. Buluta and F. Nori, Quantum Simulation, *Science* **326**, 108 (2009).
- [29] I. M. Georgescu, S. Ashhab, and F. Nori, Quantum Simulation, *Rev. Mod. Phys.* **86**, 153 (2014).
- [30] N.-N. Zhang, M.-J. Tao, W.-T. He, X.-Y. Chen, X.-Y. Kong, F.-G. Deng, N. Lambert, and Q. Ai, Efficient Quantum Simulation of Open Quantum Dynamics at Various Hamiltonians and Spectral Densities, *Front. Phys.* **16**, 51501 (2021).
- [31] B.-X. Wang, M.-J. Tao, Q. Ai, T. Xin, N. Lambert, D. Ruan, Y.-C. Cheng, F. Nori, F.-G. Deng, and G.-L. Long, Efficient Quantum Simulation of Photosynthetic Light Harvesting, *npj Quantum Inf.* **4**, 52 (2018).
- [32] X.-Y. Chen, N.-N. Zhang, W.-T. He, X.-Y. Kong, M.-J. Tao, F.-G. Deng, Q. Ai, and G.-L. Long, Global Correlation and Local Information Flows in Controllable Non-Markovian Open Quantum Dynamics, *npj Quantum Inf.* **8**, 22 (2022).
- [33] Z. Leghtas, S. Touzard, I. M. Pop, A. Kou, B. Vlastakis, A. Petrenko, K. M. Sliwa, A. Narla, S. Shankar, M. J. Hartidge, M. Reagor, L. Frunzio, R. J. Schoelkopf, M. Mirrahimi, and M. H. Devoret, Confining the State of Light to a Quantum Manifold by Engineered Two-Photon Loss, *Science* **347**, 853 (2015).
- [34] M. Malekakhlagh and A. W. Rodriguez, Quantum Rabi Model with Two-Photon Relaxation, *Phys. Rev. Lett.* **122**, 043601 (2019).
- [35] R. H. Dicke, Coherence in Spontaneous Radiation Processes, *Phys. Rev.* **93**, 99 (1954).
- [36] J. R. Schrieffer and P. A. Wolff, Relation between the Anderson and Kondo Hamiltonians, *Phys. Rev.* **149**, 491 (1966).
- [37] H. P. Breuer and F. Petruccione, *The Theory of Open Quantum Systems* (Oxford University Press, New York, 2002).
- [38] J. R. Johansson, P. D. Nation, and F. Nori, QuTiP: An Open-Source Python Framework for the Dynamics of Open Quantum Systems, *Comput. Phys. Commun.* **183**, 1760 (2012).
- [39] J. R. Johansson, P. D. Nation, and F. Nori, QuTiP 2: A Python Framework for the Dynamics of Open Quantum Systems, *Comput. Phys. Commun.* **184**, 1234 (2013).
- [40] H. J. Carmichael, *An Open Systems Approach to Quantum Optics* (Springer-Verlag, Germany, 1993).
- [41] C. W. Gardiner and P. Zoller, *Quantum Noise: A Handbook of Markovian and Non-Markovian Quantum Stochastic Methods with Applications to Quantum Optics* (Springer, Berlin, 2004).
- [42] M.-J. Hwang, P. Rabl, and M. B. Plenio, Dissipative Phase Transition in the Open Quantum Rabi Model, *Phys. Rev. A* **97**, 013825 (2018).
- [43] Q. Ai, P. B. Li, W. Qin, J. X. Zhao, C. P. Sun, and F. Nori, The NV Netamaterial: Tunable Quantum Hyperbolic Metamaterial Using Nitrogen Vacancy Centers in Diamond, *Phys. Rev. B* **104**, 014109 (2021).
- [44] H. Dong, D. Z. Xu, J. F. Huang, and C. P. Sun, Coherent Excitation Transfer via the Dark-State Channel in a Bionic System, *Light Sci Appl* **1**, e2 (2012).